

# Urban tree cover provides consistent mitigation of extreme heat in arid but not humid cities



Peter C. Ibsen <sup>a,\*</sup>, Benjamin R. Crawford <sup>b</sup>, Lucila M. Corro <sup>a</sup>, Kenneth J. Bagstad <sup>a</sup>, Brandon E. McNellis <sup>c</sup>, George D. Jenerette <sup>d</sup>, Jay E. Diffendorfer <sup>a</sup>

<sup>a</sup> U.S. Geological Survey, Geosciences and Environmental Change Science Center, Lakewood, CO, United States of America

<sup>b</sup> Department of Geography and Environmental Sciences, University of Colorado Denver, Denver, CO, United States of America

<sup>c</sup> USDA Forest Service, Institute of Pacific Islands Forestry, Hilo, HI, United States of America

<sup>d</sup> Department of Botany and Plant Science, University of California Riverside, Riverside, CA, United States of America

## ABSTRACT

Urban land cover types influence the urban microclimates. However, recent work indicates the magnitude of land cover's microclimate influence is affected by aridity. Moreover, this variation in cooling and warming potentials of urban land cover types can substantially alter the exposure of urban areas to extreme heat. Our goal is to understand both the relative influences of urban land cover on local air temperature, as well as how these influences vary during periods of extreme heat. To do so we apply predictive machine learning models to an extensive *in-situ* microclimate and 1 m land cover dataset across eight U.S. cities spanning a wide aridity gradient during typical and extreme heat conditions. We demonstrate how the cooling influence of tree canopy and the warming influence of buildings on microclimate linearly scales with regional aridity, while the influence of turf and impervious surfaces does not. These interactions lead tree canopy to consistently mitigate to air temperature increases during periods of extreme heat in arid cities, while the influence of urban tree canopy on extreme heat in humid regions is varied, suggesting that mitigation is possible, but tree canopy can also aggravate extreme heat or have no significant effect.

## 1. Introduction

Urban ecologists have studied differences between urban and rural heat characteristics (commonly known as the urban heat island phenomena) for decades, but more recent attention has been given to urban heat within cities (Buo et al., 2023; Shandas et al., 2019; Shiflett et al., 2017). Within-city urban heat research also underpins the goal of mitigating extreme urban heat, which has spurred municipalities and the U.S. Federal Government to invest over one billion USD in urban forestry (Garrison, 2021). However, the degree to which planting trees or otherwise altering urban land cover types can mitigate surface and air temperature is complex and not fully understood. For example, regional climate can moderate urban land cover's influence on urban heat (Li et al., 2019), making tree planting strategies to reduce heat potentially more effective in some cities than others depending on the regional aridity, which drives evaporative demand and therefore transpiration (Shashua-Bar et al., 2023). Periods of extreme heat can potentially reduce heat mitigation provided by trees in some cases (e.g., increasing tree death through heat stress in some species), and possibly increase heat mitigation in others (e.g., killing herbivorous pests or increasing transpiration in certain tree species) (Ossola & Lin, 2021; Winbourne

et al., 2020). As urban climate models point to more frequent and intense periods of extreme heat, the complexities of responses to extreme heat are key uncertainties needing to be resolved. Therefore, to best address urban heat at the local and continental scales, a comprehensive understanding is needed of how different land cover types influence within-city heat during typical summer climate and extreme heat conditions across regional climates.

Urban areas have extremely heterogeneous distributions of land cover types, all of which can influence urban temperatures (Cadenasso et al., 2007; Smith, et al., 2023). At neighborhood ( $\sim 10^3$  m) and micro to meso-scales ( $\sim 10^0$ – $10^3$  m) (Barlow, 2014), vegetated land covers can reduce local temperatures through an interacting mix of biophysical processes, such as trees' shading of surfaces and transpiring water from leaves, but cooling potential can vary based on available water resources (Winbourne et al., 2020). Turf, however cools air primarily through transpiration and is more limited by water availability, displaying thermal properties similar to impervious surfaces during extended dry periods (Rahman et al., 2021; Smith et al., 2023). Impervious surfaces and built structures increase temperatures through a mix of physical and anthropogenic properties, for example, road and building materials possess high heat storage capacities, and buildings act as anthropogenic

\* Corresponding author.

E-mail address: [pibsen@usgs.gov](mailto:pibsen@usgs.gov) (P.C. Ibsen).

heat sources to the urban environment (Alhazmi et al., 2022; Offerle et al., 2005). These urban land cover types also respond uniquely to regional climates, where vegetation will transpire more in arid climates and larger buildings may store more heat and have greater anthropogenic heat fluxes in warmer weather and extreme heat (due to air conditioning usage) (Alhazmi et al., 2022; Ibsen et al., 2021; Mushore et al., 2017).

Land cover influences local air temperature via modification of surface-atmosphere energy exchanges as defined by the urban energy

balance (Oke, 1982) and surface radiation budget (Grimmond et al., 2010), where available net all-wave energy and additional energy input from anthropogenic activity (e.g., combustion, metabolism) is partitioned into sensible ( $Q_H$ ) and latent ( $Q_E$ ) heat fluxes and heat stored ( $\Delta Q_s$ ) in urban surface materials. Urban land cover types all contribute differently to these energy flux factors, as well as to the surface radiation budget, where surface radiation is the sum of incoming and outgoing shortwave solar radiation ( $K_{\downarrow}$  and  $K_{\uparrow}$ ) and incoming and outgoing long wave radiation ( $L_{\downarrow}$  and  $L_{\uparrow}$ ). From meso- to neighborhood scale areas,

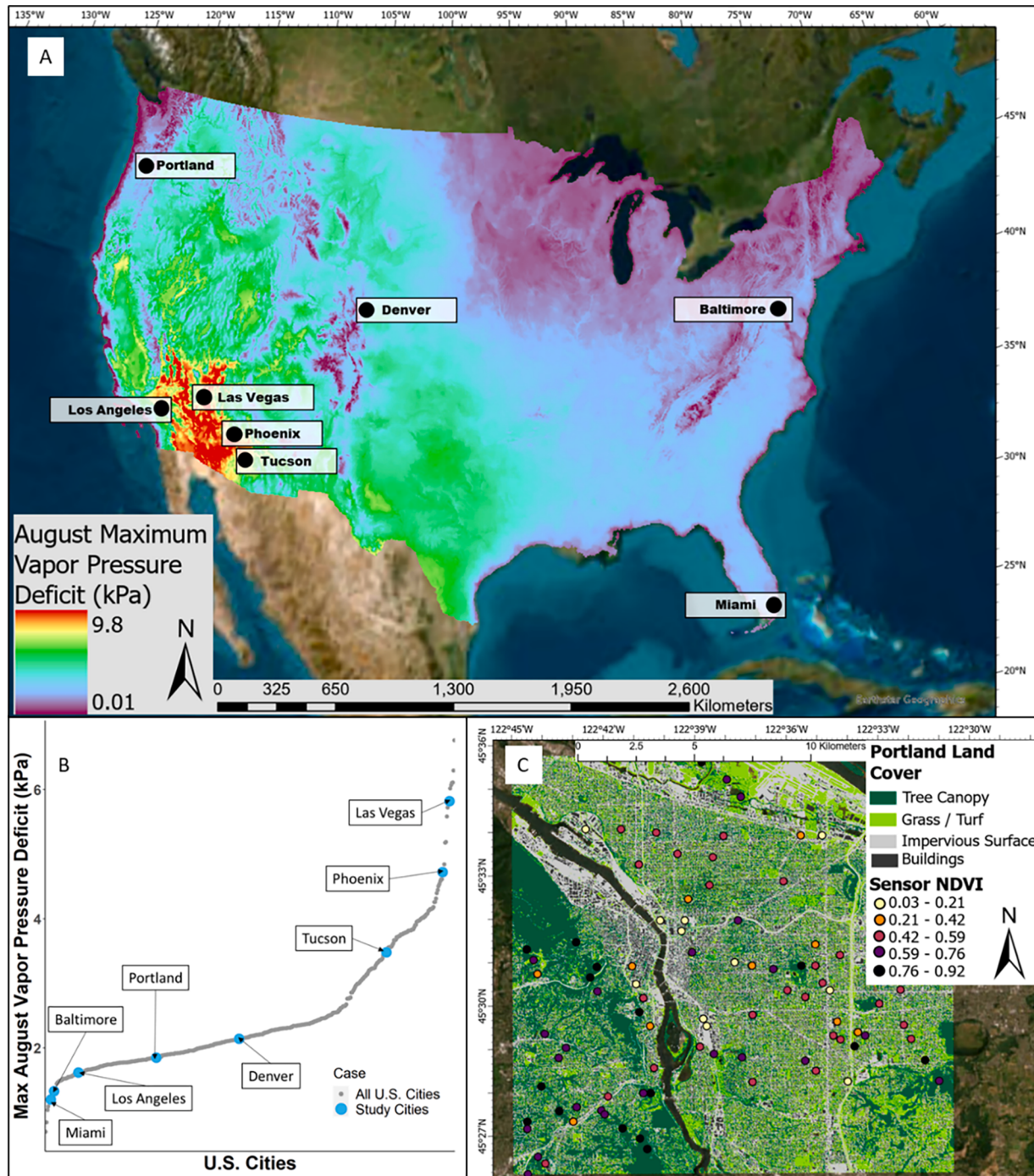


**Fig. 1.** A: The eight United States cities used in the study, with their corresponding high-resolution land cover data inlaid. The U.S. map displays the maximum vapor pressure deficit (VPD, a metric of atmospheric aridity) in the month of August. The VPD data are modeled 30-year normals (PRISM Group, 2007). B: Ranked placement of all U.S. cities with populations above 100,000 vs. mean August VPD, to display the range of the aridity gradient captured by the eight study cities. C: One study city (Portland) used as an example to display higher detail of the high-resolution land cover data, as well as the deployment of iButton sensors, stratified across a gradient of urban vegetation (displayed as the Normalized Difference Vegetation Index, NDVI).

variability in urban land cover composition creates many uncertainties in each land parcel's unique microclimate, and how the environment responds during extreme heat in different geographic regions. These variabilities are key when considering how exposure to extreme heat and the subsequent human health effects are distributed within cities.

In this paper, we quantify the spatiotemporal dynamics of within- and between-city urban heat and the capability for urban land cover types to influence how air temperature increases are mitigated or aggravated during periods of extreme heat, by synthesizing multiple high-resolution datasets, representative of a range of spatial scales. We use (1) a network of air temperature sensors representing micro-scale conditions deployed across eight cities spanning a gradient of regional mean August Vapor Pressure Deficit (VPD, a metric of atmospheric aridity) as derived from 30-year normals (PRISM Group, 2007), combined with (2) city-specific high-resolution land cover data, (3) satellite-derived land surface temperature (representing meso-scale conditions), and (4) regional climate parameters (representing macro-scale conditions). We test two hypotheses – first, tree canopy and buildings will influence local microclimate in hotter, drier regional environments more than turf and impervious surfaces due to a greater three-dimensional surface area, which will provide shade in the case of trees and increased stored heat energy in the case of buildings. Second, tree canopy and turf land covers will provide greater mitigation during extreme heat in arid cities during the day and night than in humid cities due to an increase in transpiration-derived cooling. Collectively, tests of these two hypotheses provide a clearer understanding of not only the mechanisms behind urban land cover's cooling or warming influence on the local environment in a regional climate setting, but also how heat mitigation strategies such as replacing non-vegetated land cover types with vegetation, or increasing albedo, can be enhanced during extreme heat events.

## 2. Materials and methods

### 2.1. Study locations

To capture a continental-scale gradient in regional climate, we selected eight urban extents located in the United States ("city" hereafter), covering a spectrum of regional VPD and representing multiple ecoregions (Fig. 1A & B, Table 1) (Omernik & Griffith, 2014).

While all cities in the study are major metropolitan urban areas with populations larger than 1000,000, the study extent varies by each city (Table 1). We used iButton sensors (Maxim Integrated Products, Inc. iButton Thermocron) to capture hourly air temperature at multiple locations within each extent. The exact number of sensors deployed and recovered, as well as the mean distance between each sensor is found in Table 1. We placed sensors at approximately 2 m height within trees with full canopy to prevent bias from direct radiation hitting the sensors (Terando et al., 2017). We stratified sensor distribution across a vegetation gradient, measured using the Normalized Difference Vegetation Index (NDVI) for a cloud free day in a summer month (July – September) the year prior to deployment in each city. Only one image was used for each city as NDVI was not included in the analysis but was only used to stratify sensor placement to ensure each city's deployment captured a range of urban vegetation exposures (Fig. 1C). While initial sensor deployment was binned into five NDVI categories using city-specific Jenks natural breaks. We have found this method resulted in sensors capturing a range of urban land cover types that closely resembled the total citywide fractions of land cover composition (Fig. S1 and Table 1). We reduced potential biases through removal of outliers that were three times or more than the absolute derivation around the median of the recorded day or nighttime temperatures (Leys et al., 2013). While accuracy of iButtons ( $\pm 0.5^\circ\text{C}$  depending on the specific sensor) is coarser than air temperature monitors used in meteorological towers, we are able to trade-off a decrease in accuracy for a large-scale deployment to capture greater spatial detail of different land cover types (Shi et al.,

2021). Dates of deployment and summary statistics are provided in Table 1.

Each city selected has associated high-resolution ( $\sim 1\text{ m}$ ) land cover data. We retrieved data for Baltimore, Los Angeles, Phoenix and Portland from the U.S. Environmental Protection Agency's EnviroAtlas (Pilant et al., 2020), Miami from Florida International University (Gann et al., 2020), Tucson from the Pima County Geospatial Data Portal (Pima County Geospatial Data Portal, 2023), Denver from the Denver Regional Council of Governments data portal (DRCOG Regional Data Catalog, 2018), and Las Vegas from the Nevada Division of Forestry. As the datasets were independently produced with different classification methods, we focused our study on the four types of urban land cover common to all eight cities' data and for which we had adequate coverage for intra- and inter-city comparisons: tree canopy, turf, impervious surfaces (e.g., roads, parking lots, sidewalks), and buildings.

### 2.2. Land cover influence on air temperature

We applied a 60-meter buffer surrounding each sensor and used that area to extract the land cover fractions around each sensor. A 60-m buffer has been shown to have a strong model fit when analyzing urban microclimate and land cover interactions in regards to heat mitigating ecosystem services (Crum & Jenerette, 2017; Ziter et al., 2019). We determined the total potential of each land cover type's influence on air temperature by a linear regression of the daily sensor's air temperature data at daytime (13:00–15:00 h data mean) and nighttime (01:00–03:00 h data mean) against the land cover fraction found within the buffer. For example, a single tree canopy daytime point in Fig. 2 depicts the slope coefficient for all the sensor's mean air temperature recordings within a city during daytime hours for a single day's daytime or nighttime period of the study, regressed against the tree canopy percentage within the buffer. The regression slope indicates the maximum potential influence on air temperature by that land cover type for that day specific weather pattern ( $^\circ\text{C}/\text{Fraction of Land Cover}$ ). Coefficients for each day and night of sensor deployment are then plotted against the regional VPD at time of in that city (calculated from an aggregate of the three nearest airports). We included only significant slopes in the analysis. This method has been used previously to examine the cooling efficiency of vegetated land covers on urban heat exposure (Du et al., 2024; Ibsen et al., 2021; Zhou et al., 2021), though we are also focused on the "warming efficiency" of land cover as well, resulting in four slope coefficients (one for each land cover type) for each daily daytime and nighttime period. An example of this methodology is provided in Fig. S2.

We further examined the relationship between land cover and summertime air temperature by implementing a random forest regression analysis. Land cover influences air temperature in unique ways throughout the year (Manoli et al., 2020). However, because exposure to urban heat has strong correlations to human health and mental well-being (Barboza et al., 2021; Hondula et al., 2018; Mullins & White, 2019) and as our sensor network was only deployed during summer months, we have kept our analysis focused on summertime conditions. In addition to using land cover variables as predictors, we included daytime land surface temperature (LST) as a local climate variable. We used the mean daytime LST value at 30-meter resolution from cloud-free Landsat scenes available during the summertime sensor deployments, provided by the U.S. Geological Survey (Specific image dates used found in Supplemental Table 1) (Dwyer et al., 2018). For Miami however, that were no fully cloud free images available during the study period. To keep all the City-Specific models the same, we used the least cloud-covered image and masked out any cloud-covered area. We used daytime, Landsat-derived LST for both our daytime and our nighttime models. However, previous work has found significant correlation between daytime LST and nighttime air temperature across multiple cities (Shiflett et al., 2017), as well as strong relationships between land cover types and nighttime LST when using random forest models (Logan et al.,

**Table 1**

Study city and sensor deployment dynamics, regional (three-years data of the three nearest airport meteorological towers) and local (derived from sensors used in the study) air temperature dynamics and aridity (VPD, vapor pressure deficit), and summary land cover data at the city scale (over the entire study extent) and within the 60 m buffer surrounding each sensor.

City	Baltimore MD	Denver CO	Las Vegas NV	Los Angeles CA	Miami FL	Phoenix AZ	Portland OR	Tucson AZ
<b>Study City and Region Dynamics</b>								
<b>Ecoregion (Level II)</b>								
Eastern Temperate Forest	Great Plains	North American Desert	Mediterranean California	Tropical Wet Forest	North American Desert	Marine West Coast Forest	North American Desert	North American Desert
Population (millions)	2.7	2.9	2.2	13.1	6.1	4.8	2.4	1
Mean Maximum August VPD	1.66	2.94	6.32	1.76	1.49	5.71	2.69	4.6
Dates of Sensor Deployment	07/11/2017 - 09/30/2017	07/10/2018 - 09/12/2018	06/11/2018 - 08/19/2018	06/23/2017 - 09/14/2017	07/01/2018 - 09/18/2018	06/11/2017 - 08/15/2017	06/20/2017 - 08/24/2017	06/14/2019 - 09/07/2019
Sensors Deployed/ Analyzed	100/78	90/58	90/81	100/89	88/80	100/82	100/95	90/83
Mean Sensor Distance (km)	0.842	0.978	1.418	0.564	1.053	0.940	0.880	0.945
Area of Study Extent (km <sup>2</sup> )	173.48	322.42	360.36	167.9	368.21	277.1	194.76	237.37
Land Cover Data Source	Environmental Protection Agency EnviroAtlas	Denver Regional Council of Governments Land Use Land Cover Data	Nevada Division of Forestry Urban Tree Canopy Assessment	Environmental Protection Agency EnviroAtlas	Miami-Dade County Urban Tree Cover	Environmental Protection Agency EnviroAtlas	Environmental Protection Agency EnviroAtlas	Pima County Geospatial Data Portal
<b>Temperature Summary Data</b>								
Period of Regional Climate	Jun - Sep; 2016 - 2018	Jul - Sep; 2017 - 2019	Jun - Aug; 2016 - 2019	Jun - Sep; 2016 - 2018	Jul - Sep; 2017 - 2029	Jun - Aug; 2016 - 2028	Jun - Aug; 2016 - 2018	Jun - Sep; 2018 - 2020
Median Daytime Regional Air Temperature (°C)	28.8	28.8	38.3	24.4	32	38.1	24.8	37.2
Median Nighttime Regional Air Temperature (°C)	21.1	17.2	29.4	19.3	26.7	30.6	15.6	26.7
95th Percentile Daytime Regional Air Temperature (°C)	34.4	35	43.3	29.6	33.9	42.8	33.9	41.7
95th Percentile Nighttime Regional Air Temperature (°C)	24.4	21.6	34.4	22.8	28.5	35	20	31.1
Median Daytime Local Air Temperature (°C)	28.1	30.5	40.5	28.6	31.5	40.5	27.1	40
Median Nighttime Local Air Temperature (°C)	20.7	18.1	30.1	20.1	26.5	31	17.1	27.5
95th Percentile Daytime Local Air Temperature (°C)	35.1	37	46	35.7	35.1	46	36.1	44.6
95th Percentile Nighttime Local Air Temperature (°C)	26.5	23.5	34.7	25.1	28.5	35.5	23.1	31.5
<b>Summary Land Cover Data</b>								
Tree Canopy Percentage (Citywide scale)	28.6	12.7	10.1	20.1	14.5	6.5	27.3	17.1
Turf/Grazing Percentage (Citywide scale)	16.5	22.1	5.7	10.1	18.5	7.6	22.3	0.02

(continued on next page)

**Table 1 (continued)**

City	Baltimore MD	Denver CO	Las Vegas NV	Los Angeles CA	Miami FL	Phoenix AZ	Portland OR	Tucson AZ
Impervious Surface Percentage (Citywide scale)	36.3	38.7	46.2	40	29.1	33.9	30.1	23.6
Building Surface Percentage (Citywide scale)	16.1	16.2	18	25	17	14.6	14	13.2
Median Tree Canopy Percentage (60 m surrounding sensor)	19.1	11.4	13	24.5	17.1	7.9	21.1	18.1
Median Turf/Grass Percentage (60 m surrounding sensor)	5.9	15.8	6.4	8.8	14.1	6.8	18.9	1.2
Median Impervious Surface Percentage (60 m surrounding sensor)	44.3	45	41.3	39.5	41.9	42.1	27.3	30
Median Building Surface Percentage (60 m surrounding sensor)	13.3	13.3	2.6	19.9	9.6	8.9	13.4	2.4

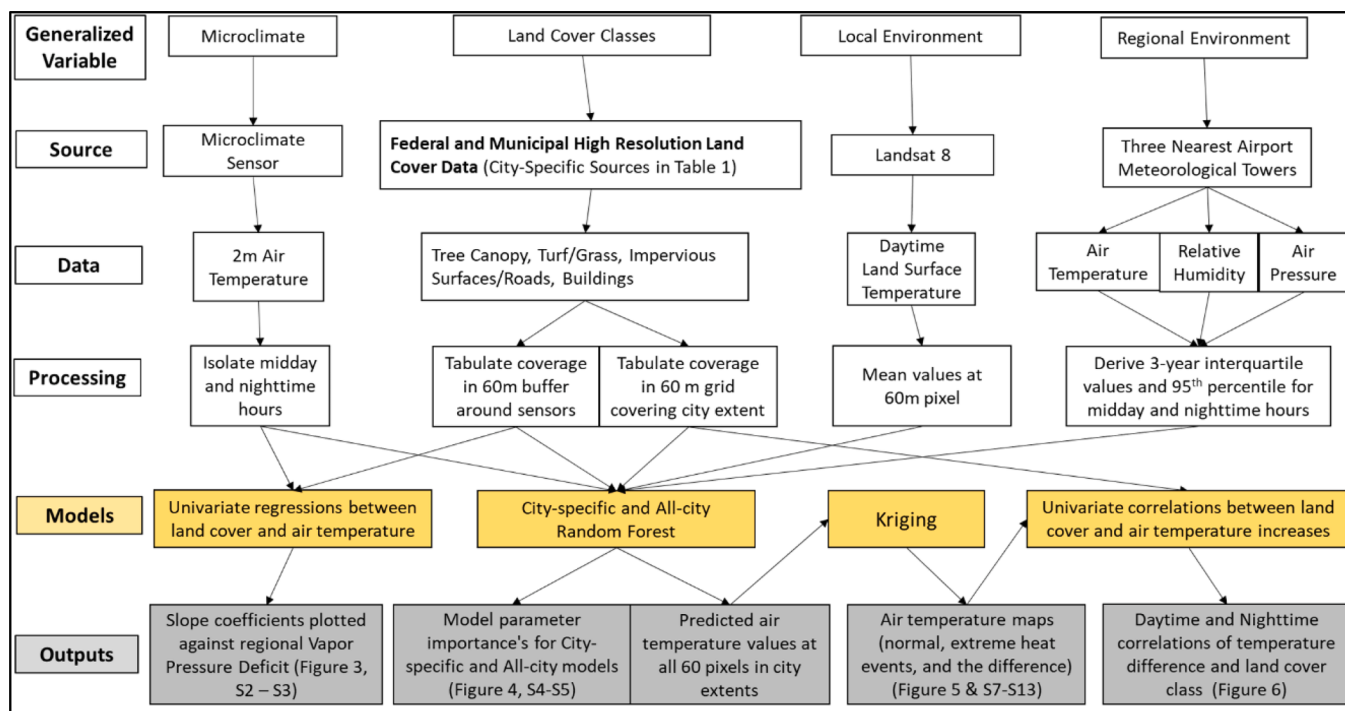


**Fig. 2.** Model flow diagram depicting all variables, data sources, generalized processing, models, and main outputs described in the manuscript. Modified from Ibsen 2022 (Ibsen et al., 2022).

2020). Prior research thus suggests that including daytime LST and urban land cover in a nighttime model can still provide strong prediction accuracy.

To represent regional climate, we retrieved the dry bulb temperature, wind speed, relative humidity, and atmospheric pressure from the three closest airport meteorological stations to each study city, during the three-year period around each city's sensor deployment, specific to the hours of analysis (midday – 13:00–15:00 – and midnight – 01:00 to 03:00). This three-year window enables representative regional climate

variability during the deployment, without including data from far beyond the study conditions. We created two All-City and sixteen City-Specific random forest models to model the influence of predictors on daytime and nighttime temperature. The All-City model uses all the parameter data from the eight cities (four land cover types, three regional climate parameters, and daytime LST), and each model was tuned to determine the optimal number of variables used at each node. However, we maintained consistency across models by not adjusting the number of parameters to improve fit as our primary objective was to

compare results across cities using the same inputs. We divided our dataset randomly, allocating 70 % of the data to train the model with the sensor air temperature values as the response variable, and the remaining 30 % of data was reserved for testing the trained model's performance. The 70/30 training/testing split ratio was selected based off prior usage in urban land cover and urban heat models (Gardes et al., 2020; Liu et al., 2024; Mohammad et al., 2022). Feature importance of parameters was determined by the percent increase in mean square error (%IncMSE). This metric measures how prediction accuracy changes when a parameter is excluded, thus a higher %IncMSE implies greater overall importance, as removing that parameter would result in greater model error. The combination of using sensor and land cover data in machine learning models to determine relative variable influence and predict wider spatial temperature dynamics is well established in the modern urban climate literature (Duncan et al., 2019; Lau et al., 2023; Shandas et al., 2019). Model fit is determined by the adjusted  $R^2$  of the linear regression between the test predicted values of the 30 % and the corresponding observed sensor air temperature values. We used the same training and test methods to produce City-Specific models for each city. The training data size was 89,046 and 92,424 observations for day and nighttime, respectively, in the All-City Model and ranged from 7734 to 15,299 observations in the City-Specific Models.

### 2.3. Extreme heat event analysis

We derived air temperature maps of typical summer climate and an extreme heat condition in our study cities by using the City-Specific random forest models described in the previous section. Our "typical" summer climate parameter set represented the mean interquartile values of air temperature, relative humidity, and wind speed over a three-year period surrounding the year of sensor deployment for that city, and an "extreme heat" regional climate parameter set, which uses the 95th percentile of the same parameters. To create city-wide values, we extracted the land cover fractions and mean daytime LST within 60 m grid pixels covering the city. We then used these 60 m land cover fractions and mean daytime LST value as local area parameters in the random forest model. The regional climate and local area parameters served as a test dataset, for which we used the model trained on the sensor's air temperature to predict air temperature for all 60 m grid pixels in each city. We then interpolated predicted air temperature values for each city using an Ordinary Kriging model. The specific semivariogram parameters selected by fitting exponential, spherical, and Gaussian models to modeled air temperature results for each city, climate condition (typical, extreme heat), and time of day (daytime, nighttime). The nugget, partial sill, and range value used in the kriging were selected from the semivariogram fit with the lowest sum of squared error value (Table S2). We mapped results from kriging in ArcGIS Pro 3.0.3 (ESRI Inc) and considered all points within a range of 600 m, acting as a blending factor to approximate wind mixing (Lonsdorf et al., 2021). We calculated land cover types' influence on air temperature increases during periods of extreme heat by taking the correlation of the difference between predicted air temperature values during modeled extreme heat events and the modeled typical climate values, and the fraction of land cover type within the citywide 60-meter pixels, at both day and nighttime hours. To visualize the spatial pattern of land cover influence on temperature increases, we used correlation coefficients for each land cover type/city combination as a scaling factor for the land cover fraction found in each pixel. A model flow diagram is provided in Fig. 2.

As we are using correlations between land cover and air temperature increases, we can describe how closely related the land cover types are with increases or decreases in air temperature, but not the effect size of that relationship. We completed all statistical modeling analysis in R Version 4.2.2 (RStudio Team, 2020) using the following packages (Semivariogram fitting and cross validation – package gstat; random forest – package randomForest; extreme heat slope comparison –

package lsmeans) (Lenth, 2016; Liaw & Wiener, 2002; Pebesma, 2004). All data used in analysis is openly available at ([Ibsen et al., 2024](#)).

## 3. Results

### 3.1. Regional drivers of urban land cover-air temperature influence

Across most cities, buildings and impervious surfaces were correlated with increasing air temperature during day and night, with buildings contributing a mean maximum warming potential of 4.7 °C and 3.9 °C and impervious surfaces warming 2.6 °C and 2.4 °C during the day and night, respectively. On the other hand, turf and tree canopy were correlated with decreasing urban air temperature, with tree canopy contributing a mean maximum cooling potential of 4.2 °C and 3.4 °C and turf cooling 3.2 °C and 3.0 °C during the day and night, respectively (Fig. S3). Across the continental aridity gradient, warming produced by buildings and the cooling produced by tree canopy scaled linearly with the regional VPD. By contrast, the warming and cooling produced by impervious surfaces and turf remain relatively flat across the aridity gradient, especially during the day (Fig. 3). In daytime hours, we found regional aridity explained the majority of variance in both buildings and tree canopy's influence on air temperature, and a very small amount of variance in turf's air temperature influence (Buildings:  $R^2 = 0.58$ ,  $p < 0.001$ . Tree Canopy:  $R^2 = 0.61$ ,  $p < 0.001$ ; Turf:  $R^2 = 0.02$ ,  $p = 0.03$ ). Aside from buildings, the relationships between land cover-induced temperature moderation increased during the nighttime (Buildings:  $R^2 = 0.56$ ,  $p < 0.001$ ; Impervious Surface:  $R^2 = 0.22$ ,  $p < 0.001$ ; Tree Canopy:  $R^2 = 0.66$ ,  $p < 0.001$ ; Turf:  $R^2 = 0.17$ ,  $p < 0.001$ ) (Fig. 3). The regional influence in daytime air temperature modification can be interpreted as, for each unit increase in daytime VPD, the maximum cooling potential of tree canopy increases by 0.63 °C, and maximum warming potential of buildings increases by 0.53 °C. During nighttime hours these VPD-driven increases to temperature modification are increased, where tree canopy's maximum cooling potential increased 1.33 °C for every kPa increase to VPD, and buildings' maximum warming potential increased by 1.20 °C.

### 3.2. Urban air temperature predictive modelling

We built an All-City random forest model through the combination of regional and local climate dynamics as well as local land cover characteristics of all eight study cities. This model was able to explain most of the variation in daytime and nighttime air temperature at the continental scale (Daytime  $R^2 = 0.96$ , Nighttime  $R^2 = 0.98$ ) (Fig. S4A & C). When focusing on individual city predictions, the All-City algorithm displayed more variability in model-fit across each city, though overall model-fits were better during nighttime hours (Fig. S4B & D). These values were close to the predicted values when building similar models on each city independently (City-Specific models; Fig. S5). While our most humid city (Miami) exhibited the lowest amount of air temperature variability explained by our land cover variables, there was no significant trend across all cities dependent on regional aridity.

Overall, when evaluating the importance of variables in our All-City model, we found regional and local climate characteristics were the strongest predictors of daytime temperatures, while during nighttime regional climate parameters were the strongest air temperature predictors, and local climate was the weakest predictor (Fig. 4A). Specifically, regional climate parameters of wind speed and air temperature displayed high importance in increasing model accuracy when predicting local air temperature variation in both our daytime and nighttime All-City models. In the All-City model, land cover parameters had moderate importance in both day and night; though during the day, the green land cover types of tree canopy and turf exhibited greater importance than the grey land cover types of impervious surface and buildings (Fig. 4A). We observed more variability in parameter importance when looking at individual City-Specific random forest models

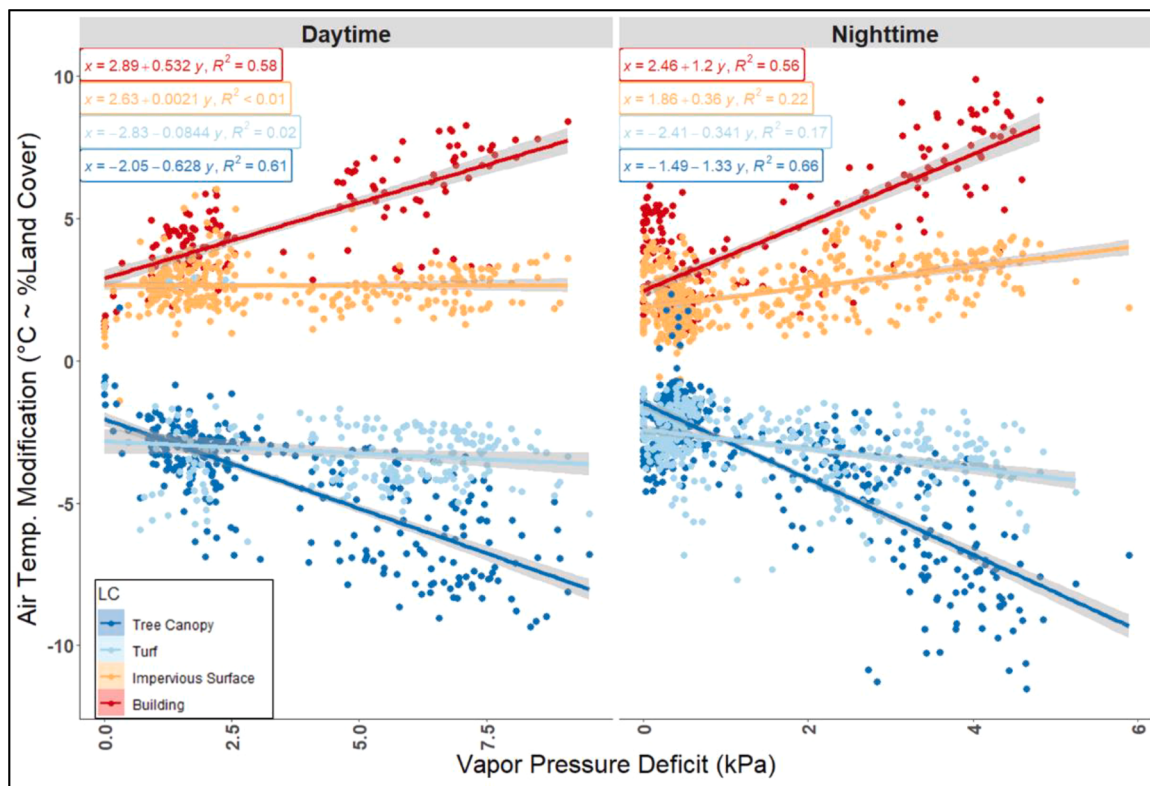


**Fig. 3.** Air temperature modification of urban land covers as a factor of regional Vapor Pressure Deficit across all eight study cities during daytime (13:00–15:00) h, and nighttime (01:00–03:00) h. Each point represents the slope coefficient of a significant linear regression between the color-specified land cover and the air temperature recorded across a network of microclimate sensors within one of the study cities. Regression lines are color coded to a specific urban land cover type, and shading represents the standard error. Line equations, adjusted  $R^2$ , and p values of the land cover regressions are provided in top left.

(Fig. 4B). Importance of land cover variables significantly increased in more arid cities during the day and night (Daytime: p value = 0.002, adjusted  $R^2$  = 0.26; Nighttime: p value = 0.015, adjusted  $R^2$  = 0.15; Fig. S6).

### 3.2. Land cover influences on extreme heat events

Through predictive modelling, we mapped air temperature during plausible average summer days and extreme heat events. This mapping allowed us to calculate the increase in air temperature at every 60 m pixel within our study cities during these extreme heat events as compared to a typical summer climate. The mapped outputs during the day and night for Baltimore are provided in Fig. 5 and similar figures for the other seven cities are available in the supplement (Figs. S7–S13).

We then correlate the temperature increase during extreme heat events by fraction of land cover within a 60 m grid cell. A significant positive correlation indicates that during heat events, the air temperature increases more rapidly as land cover type increases, while a negative correlation indicates that air temperature increases less rapidly as a land cover type increase. We found that vegetated land cover fractions in Tucson, Phoenix, and Las Vegas were negatively correlated with temperature increase. Tree canopy, in particular, was strongly negatively correlated to temperature increases during the day and night in those three cities (Fig. 6). Similarly in the two most arid cities (Las Vegas and Phoenix), the impervious surface fractions were positively correlated with temperature increase. Unlike the arid cities, more humid cities exhibited a greater variability in the correlation between temperature increase and land cover fraction depending on land cover type and time of day. For example, during the day in Portland, heavily treed areas experience a greater increase in daytime and nighttime air temperatures during heat events compared to areas with greater percentages of buildings (Fig. 6).

## 4. Discussion

Throughout Europe (Maes et al., 2021) and the United States (United State White House, 2023), major investments are being made to increase urban vegetation with a focus on heat mitigation. However, our results provide clear evidence that simply adding greenness is not a one-size-fits-all approach to urban heat management. Finding that the cooling effects of vegetated land cover types and the warming effects of built structures are modified by regional climate suggest that the biomechanical and physical processes that drive air temperature mitigation are city-specific, so city-specific heat mitigation planning is needed. We found that increasing tree canopy provides air-cooling benefits in all our study cities (Fig. S3), though the arid cities had the largest effects. A main reason for these differences of tree canopy cooling in arid cities is the additive properties of shading and evapotranspiration on both air and surface temperatures. Evapotranspiration is determined by the local aridity (Sulman et al., 2016), and is the likely cause of our results: in cities with greater regional aridity, tree canopy provides greater heat mitigation due to a subsequent increase in latent heat flux (the energy used to evaporate transpired water) while also reducing surface temperature through shading (Winbourne et al., 2020).

Interestingly, this effect is prominent in tree canopy but not turf. This is primarily due to the structural properties of trees versus turf. While turf evapotranspiration is found to be higher in arid cities (Grijseels et al., 2023), it is less likely to impart cooling at a height relevant to humans (Crum & Jenerette, 2017). While tree canopy not only provides cooling closer to the height of an average human, but trees' size also means there is a double benefit of shading and increasing total transpiration as trees become taller. Given that water for irrigation is a limited resource, especially in arid environments (Jenerette et al., 2011), our results also underscore how focusing on trees in greenspaces over irrigated turf in arid cities can increase the heat mitigation



**Fig. 4.** Model parameter importance outputs from All-City (A) and City-Specific (B) random forest models. The All-City model analysis includes all eight study cities together within the same model, with models run using daytime and nighttime data, while the City-Specific model analyzes each city separately, with models run using daytime and nighttime data. Model inputs are grouped by type (e.g., regional climate, local climate, land cover). Model importance is measured as the percent increase in mean squared error, which is a measure of how much the model accuracy decreases when leaving out that variable.

potential of urban green infrastructure while reducing municipal water loss.

While tree canopy can require less irrigation than turf, supplemental irrigation is still necessary to maintain current tree canopy in many of these arid cities. Moreover, while vegetation in cities may have the ability to transpire under higher VPD than rural plants (Winbourne et al., 2020; Yuan et al., 2019), alleviating atmospheric drought stress, recent work in urban Sydney, Australia, found that during a two-week heat wave even well-watered trees, which did not display any hydraulic failure, still experienced leaf death (Marchin et al., 2022). The die-back was also partially dependent on the biogeographic origins of the planted tree species, where precipitation during the driest month of the species geographical range was significantly correlated with crown die-back. This indicates the important role of well-trained urban foresters in selecting the right species to withstand extreme heat, and greater research into the vulnerability of urban tree species to heat vulnerability.

#### 4.1. Urban land cover and the urban energy balance

We can interpret observed land cover-air temperature relations in the framework of the urban surface energy balance and radiation

budget. Leaf area index (the amount of leaf per unit ground area, LAI) from complex three-dimensional tree canopies means greater active surface area for  $Q_E$  from tree leaves relative to turf. There is also additional cooling benefit from shading by tree canopies, which is not available for turf.

As regional aridity increases, we found that greater cooling is associated with tree cover during both daytime and nighttime periods (Fig. 3). During daytime, as regional VPD increases,  $Q_E$  is enhanced, at the expense of  $Q_H$  and  $\Delta Q_S$ , by greater vegetation-atmosphere moisture gradients. Overnight, in all regional climate settings, vegetated areas tend to cool faster than built areas in part due to a lack of  $Q_H$  and  $\Delta Q_S$  sources that contribute to warmer nighttime temperatures in more densely built areas (Oke et al., 2017). With low humidity, vegetated areas may cool down even more rapidly than built-up areas due to lack of moisture and cloud cover in the overlying atmosphere. A drier atmosphere reduces absorption and re-radiation of longwave energy at city-wide scales and thus enhances differential radiative cooling rates between surface types. By contrast, in humid regions, greater shortwave radiation received at the surface reduces differential radiative cooling rates and dampens micro-scale temperature variations (Oke et al., 2017), resulting in the high variability of land cover correlations with heat increases in humid cities (Fig. 6).

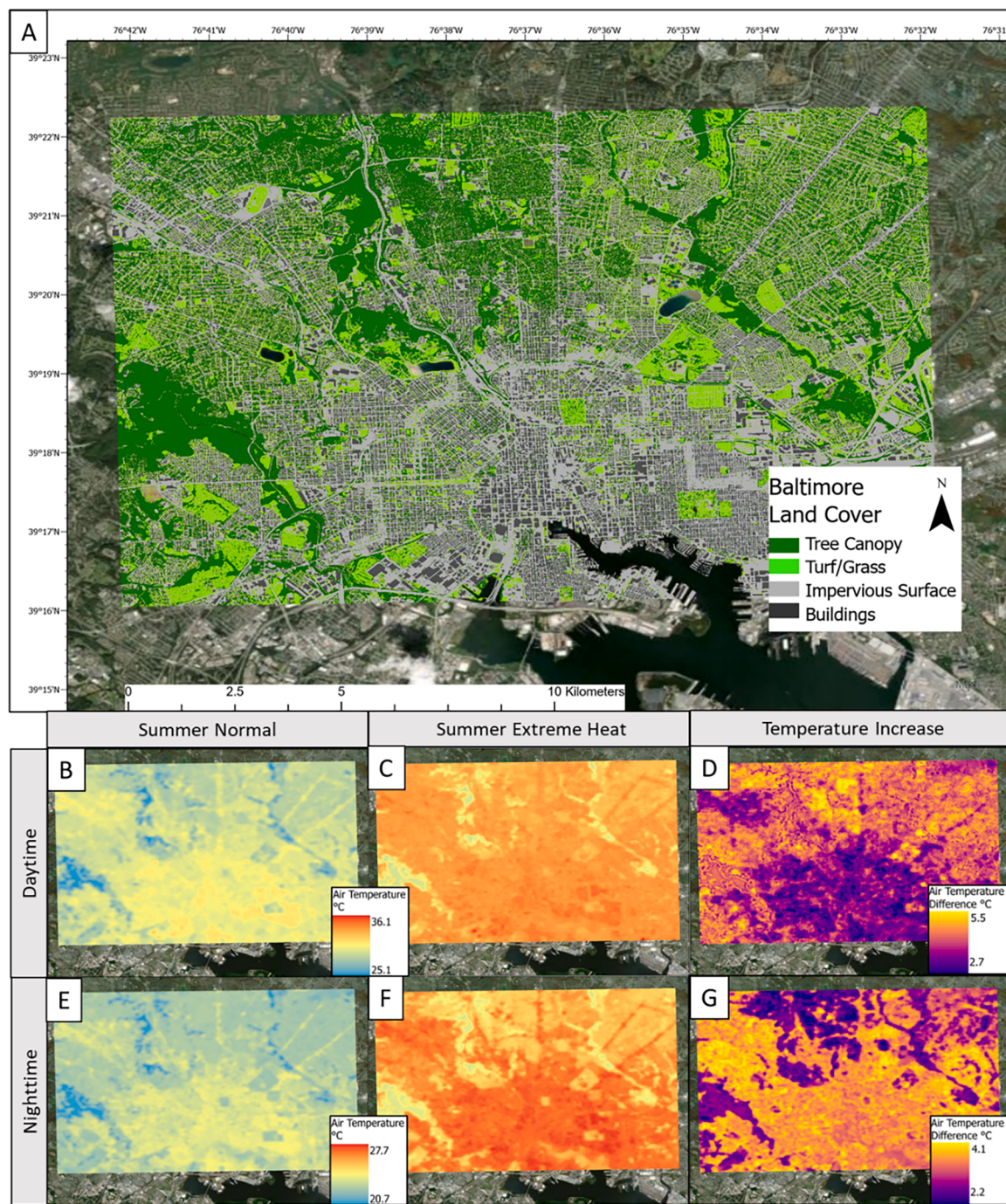


**Fig. 5.** Study city land cover and predictive temperature modelling results for Baltimore, MD. (A) The sampled study extent displaying the high-resolution (1 m) land cover data input to our predictive model. Mapped All-City Model results for (B) typical daytime (13:00–15:00) summer climate conditions, (C) daytime summer extreme heat conditions, (D) the difference between daytime extreme heat and the typical (E) nighttime (01:00–03:00) summer climate conditions, (F) nighttime summer extreme heat conditions, (G) the difference between nighttime extreme heat and the typical conditions.

As building land cover increases, greater building surface area preferentially channels energy towards  $Q_H$  and  $\Delta Q_S$  in all regional climate settings during dry, daytime conditions. Buildings are also a anthropogenic heat source to the atmosphere (Alhzam et al., 2022). In more arid regions, the heating impact of buildings appears enhanced, due to greater cooling magnitude from vegetation in areas with low building and high vegetation land cover fractions (Fig. 3). Building and vegetation land cover fractions are inversely correlated, and linear slopes between building land cover and air temperature show positive correlations in dry climates because of enhanced cooling in low

building/high vegetation land cover locations. In more humid areas, the vegetation cooling impact is muted in low building/high vegetation locations, resulting in flatter building land cover-air temperature slopes. These two dynamics—trees increasing  $Q_E$  in arid areas and buildings acting as large batteries of heat storage—further reinforce the findings of Li et al. (2019), which provide evidence that urban heat intensity is strongly driven by differences in the land cover types' capacity to evaporate water (e.g., impervious surfaces vs. vegetation) rather than aerodynamics of urban boundary layers (Li et al., 2019).

Overnight,  $\Delta Q_S$  and  $Q_F$  releases from buildings generally promote

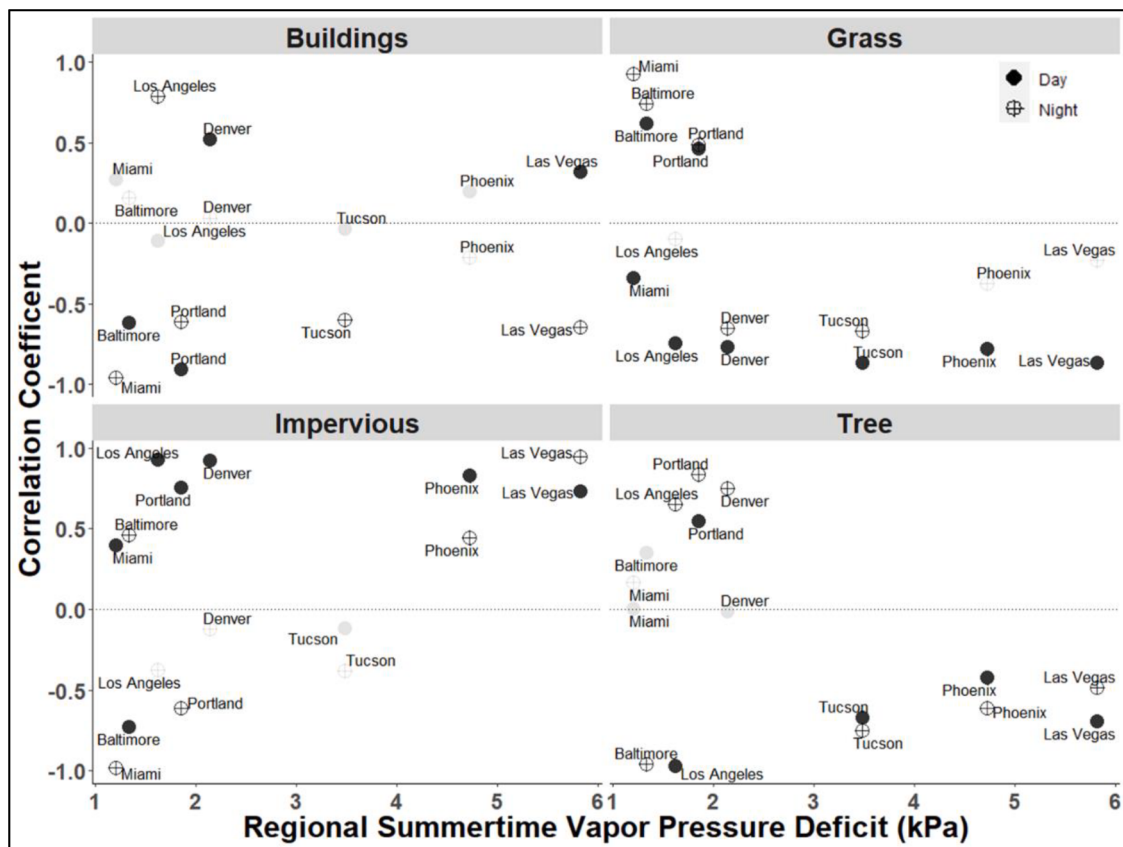


**Fig. 6.** Pearson correlation coefficients for each urban land cover type and air temperature increases occurring during modeled days and nights of extreme heat. Correlation coefficients from the relationship between land cover fraction and the amount air temperature increased during modeled extreme heat periods are plotted against the regional mean summertime vapor pressure deficit for each study city during daytime and nighttime hours. Negative values thus imply that the land cover type provides heat mitigation during extreme heat events, while positive values imply that the land cover type aggravates heat during extreme events. Non-significant correlations are greyed out. Significance determined at  $p \leq 0.05$ .

elevated micro-scale temperatures relative to areas dominated by other land cover types in all climate settings (Oke et al., 2017). Additionally, relatively flat impervious and turf surfaces have greater sky-view factor compared to complex three-dimensional street-canyon and building configurations, and thus experience more rapid cooling due to long wave radiation energy losses (Oke et al., 2017). As impervious surfaces generally have higher  $\Delta Q_s$  than turf, we can see the steeper slopes in impervious surface warming versus turf cooling in Fig. 3. In more arid regions, this overnight cooling mechanism may be enhanced due to reduced  $L^-$  resulting from less water vapor in the overlying atmosphere. As described earlier, this likely results in more rapid cooling of low building/high vegetation areas (i.e., steeper building-air temperature slopes) in arid regions relative to humid regions (i.e., flatter building-air temperature slopes).

#### 4.2. Land cover types' influence on extreme heat events

We predicted extreme heat values within each study city to map the spatial variance in extreme air temperature and quantify the mitigation or aggravation of air temperature warming provided by each land cover type. The variability in land cover types' influence on increasing temperature during extreme heat in humid cities shows that certain communities are at added risk during extreme heat scenarios. For example, the 2021 heat wave that broke records across northwestern North America appears to have been an anomalous event (Thompson et al., 2022), yet recent work points to regional humidity as having exacerbated its associated atmospheric conditions, resulting in the extreme heat at the surface that lingered for days (Schumacher et al., 2022).

Moreover, our finding of tree canopy providing greater heat mitigation bolsters recent work finding that when controlling for regional climate, more temperate mesic cities experience greater increases in heat exposure during heat waves compared to hot arid cities (Hu et al., 2023).

Our data show that vegetated surfaces are more associated with increasing air temperature during extreme heat events in the northwestern City of Portland, potentially due to the high humidity and denser tree canopy resulting in increased absorption of longwave energy. These results underscore that land cover conversions from grey to green infrastructure are only a part of an urban heat-mitigation toolkit. In more temperate cities where extreme heat is less common, fewer households are prepared with air conditioning to deal with extreme heat, and those that have air conditioning are predominantly higher-income (Romitti et al., 2022). Our results reflect the recent trend of more temperate cities in higher latitudes building cooling centers to protect underserved populations from extreme heat (Kim et al., 2021). Results shown in Fig. 6 display how land cover either aggravates or mitigates increases in air temperature during extreme heat, not how a land cover is correlated with air temperature alone.

Notably, some variability in the correlation between land cover and extreme heat-derived air temperature increases found in humid cities may also be a function of other regional and local dynamics not included in our models. For example, we found no clear pattern in buildings' influence on extreme heat-derived temperature increase during day or night, which is counterintuitive to sensor data that showed increases in building-derived warming in arid climates. While buildings do increase the  $Q_H$  in concordance with their height, large buildings also shade surfaces and alter wind flow patterns within the city (Alhazmi et al.,

2022; Tian et al., 2023), and wind speed was a very strong model parameter in both our day and night predictive models (Fig. 4A). In recent years, LIDAR data have become available for more cities, which has been used to model the effects of shade in urban heat models (Buo et al., 2023), and in some cases, the shade cast by buildings reduces the surface temperature increases caused by building envelope (area and height) by approximately 50 %, with variability also depending on building aspect (Park et al., 2021). Recent studies that select cities with LIDAR data are able to include building height, tree canopy height as well as Sky View Factor (a metric of potential shading) in their heat wave models (Hu et al., 2023). As these data sources become more common, such as the recent application of the U.S. Geological Survey (USGS) 3D Elevation Program (Snyder, 2012) to model building height in multiple United States cities they will prove useful to further resolving the complexities of the urban energy balances, adding greater nuance to the models of urban air temperatures.

Our air temperature models suggest that maximizing the benefits of heat mitigation ecosystem services from urban land cover change (i.e., tree planting) will largely depend on the regional climate. Replacing buildings and impervious surfaces with tree canopy in arid to semi-arid cities could provide both the largest heat mitigating services and add the most resistance to extreme heat targeted to areas where the current land cover is more associated with aggravating heat during extreme heat days (Fig. 5D & G). However, tree selection for heat and drought tolerance and water needs are important considerations and tradeoffs. While not a focus in this study, heat could also be mitigated through increasing the albedo of impervious surfaces (Smith et al., 2023). Increasing impervious surfaces' albedo could be especially useful in humid cities where impervious surface warming has an equal or stronger effect size compared to tree-derived cooling, such as in Miami or Baltimore, as well as potentially dampening the extreme heat aggravating aspects of impervious surfaces.

In other cities, maps of increases in temperature correlated with land cover can provide guidance for determining areas of risk during extreme heat. These areas are not necessarily the hottest in the city, but they are areas which will undergo the largest change in temperatures. As interest in increasing heat mitigation projects in cities grows, and as this interest aims to direct on-the-ground mitigation activities to populations with the greatest need, these results can help guide future urban planning. Moreover, as more cities produce high-resolution land cover and air temperature data, these models can help guide the development of additional high-resolution models showing how vegetation and the built environment affect within-city temperatures across the globe.

#### 4.3. Limitations of interpretation

In interpreting our results, we note two main limitations that can guide future research. First, we used linear regressions of each land cover and sensor-recorded air temperature and extracted any significant slope of that regression to represent the magnitude of land-cover moderation. While recent studies have shown land cover classes like impervious surface have a linear relationship with air temperature, others like tree canopy can have a non-linear relationship, where a threshold amount of tree canopy is required before temperature becomes modified (Ziter et al., 2019). Conversely, Alonzo et al., 2021 displayed linear effects of tree canopy on air cooling, and non-linear warming coming from impervious surfaces (Alonzo et al., 2021). The relationship complexities at the scale at which tree canopy density reduces air temperature deserve further analysis, especially when considering how different tree species may also significantly affect temperature mitigation (Rahman et al., 2020). While these relationships are complex, we ultimately used linear relationships for all land cover types. Our research aim was to compare land cover types' effects on air temperature across and within cities, and maintaining a standardized functional form of analysis helped us achieve that goal.

Secondly, while the choice of a 60 m scale of our analysis has been

corroborated as a suitable spatial scale to examine the effects of urban land cover on temperatures, our study does not expand into further scales of analysis. Alonzo et al. (2021) found a similar spatial scale (90 m) having the strongest model fit when analyzing the effects of tree canopy and impervious surface on afternoon air temperature anomalies. However, in their study the model fit for evening anomalies was strongest at a 200 m scale. To keep our daytime and nighttime results comparable we have kept the spatial scale of analysis the same for both. A different spatial scale of analysis though may add explanation to why in Portland turf has a warming effect on air temperature (Fig. S3). This effect does not match with the other cities in the study, nor to the current literature on turf or grass's influence on air temperature. A future multi-city analysis of analytical spatial scale variability on land cover's influence on air temperature could prove useful in explaining this finding.

#### 5. Conclusions

Our study investigated how ubiquitous urban land cover types influence local air temperatures, as well as how those land cover types mitigate or aggravate increases in air temperature during periods of extreme heat. We found overwhelmingly that the cooling effects of tree canopy and the warming effects of building density increase with regional aridity, while the more "two-dimensional" land covers of grass and impervious surfaces provide generally consistent cooling and warming, respectively. Tree canopy does mitigate heat in all study cities, but because the extent of that mitigation is dependent on regional aridity, irrigation is crucial for maintaining those heat mitigating services. Our study also displayed how regional aridity not only increases the cooling potential of tree canopy, but also that tree canopy can mitigate increases in already warm temperatures in arid cities during periods of extreme heat. However, these consistent arid-city patterns of how land cover mitigates or aggravates extreme heat found break down in humid cities. These results imply how in more humid cities, the land cover effects on extreme heat are complex, and it is important to consider city-specific complexity when planning urban land conversions to combat urban heat exposure.

#### Disclaimer

Any use of trade, firm, or product names is for descriptive purposes only and does not imply endorsement by the U.S. Government.

#### CRediT authorship contribution statement

**Peter C. Ibsen:** Writing – review & editing, Writing – original draft, Visualization, Validation, Project administration, Methodology, Investigation, Formal analysis, Data curation. **Benjamin R. Crawford:** Writing – review & editing, Writing – original draft, Conceptualization. **Lucila M. Corro:** Writing – review & editing, Methodology, Formal analysis, Data curation. **Kenneth J. Bagstad:** Writing – review & editing, Conceptualization. **Brandon E. McNellis:** Writing – review & editing, Methodology, Conceptualization. **George D. Jenerette:** Writing – review & editing, Resources, Methodology, Conceptualization. **Jay E. Diffendorfer:** Writing – review & editing, Supervision, Resources, Investigation, Conceptualization.

#### Declaration of competing interest

The authors declare the following financial interests/personal relationships which may be considered as potential competing interests: Peter Ibsen reports financial support was provided by US Geological Survey Climate Research and Development Program. Peter Ibsen reports financial support was provided by US Geological Survey - Community for Data Integration. Peter Ibsen reports financial support was provided by National Science Foundation. Jay E. Diffendorfer reports financial

support was provided by US Geological Survey Climate Research and Development Program. Kenneth J. Bagstad reports financial support was provided by US Geological Survey Land Change Science Program. G. Darrel Jenerette reports financial support was provided by National Science Foundation. Peter Ibsen reports a relationship with US Geological Survey that includes: employment. Kenneth Bagstad reports a relationship with US Geological Survey that includes: employment. Jay Diffendorfer reports a relationship with US Geological Survey that includes: employment. Lucila Corro reports a relationship with US Geological Survey that includes: employment. If there are other authors, they declare that they have no known competing financial interests or personal relationships that could have appeared to influence the work reported in this paper.

## Data availability

Data used in the analysis and all tabular data can be accessed through USGS ScienceBase at <https://www.sciencebase.gov/catalog/item/664fb9c9d34e702fe8748151>.

## Acknowledgments

We acknowledge and thank the United States Forest Service's Denver Urban Field Station (DUFS) as collaborative urban research group where preliminary results were first shared and discussed. Jeremy Havens of the USGS assisted with image creation.

## Supplementary materials

Supplementary material associated with this article can be found, in the online version, at [doi:10.1016/j.scs.2024.105677](https://doi.org/10.1016/j.scs.2024.105677).

## References

- Alhazmi, M., Sailor, D. J., & Anand, J. (2022). A new perspective for understanding actual anthropogenic heat emissions from buildings. *Energy and Buildings*, 258, Article 111860. <https://doi.org/10.1016/j.enbuild.2022.111860>
- Alonso, M., Baker, M. E., Gao, Y., & Shandas, V. (2021). Spatial configuration and time of day impacts the magnitude of urban tree canopy cooling. *Environmental Research Letters*. <https://doi.org/10.1088/1748-9326/ac122>
- Barboza, E. P., Cirach, M., Kholomenko, S., Jungman, T., Mueller, N., Barrera-Gómez, J., et al. (2021). Green space and mortality in European cities: A health impact assessment study. *The Lancet Planetary Health*, 5, e718–e730. [https://doi.org/10.1016/S2542-5196\(21\)00229-1](https://doi.org/10.1016/S2542-5196(21)00229-1)
- Barlow, J. F. (2014). Progress in observing and modelling the urban boundary layer. *Urban Climate*, 10, 216–240. <https://doi.org/10.1016/j.uclim.2014.03.011>
- Buo, I., Sagris, V., Jaagus, J., & Middel, A. (2023). High-resolution thermal exposure and shade maps for cool corridor planning. *Sustainable Cities and Society*, 93, Article 104499. <https://doi.org/10.1016/j.scs.2023.104499>
- Cadenasso, M. L., Pickett, S. T. A., & Schwarz, K. (2007). Spatial heterogeneity in urban ecosystems: Reconceptualizing land cover and a framework for classification. *Frontiers in Ecology and the Environment*, 5, 80–88. [https://doi.org/10.1890/1540-9295\(2007\)05\[80:SHIUER\]2.0.CO;2](https://doi.org/10.1890/1540-9295(2007)05[80:SHIUER]2.0.CO;2)
- Crum, S. M., & Jenerette, G. D. (2017). Microclimate variation among urban land covers: The importance of vertical and horizontal structure in air and land surface temperature relationships. *Journal of Applied Meteorology and Climatology*, 56, 2531–2543. <https://doi.org/10.1175/JAMC-D-17-0054.1>
- DRCOG Regional Data Catalog, (2018). Land use land cover pilot project section 12 2018 [WWW document]. URL [data.drcog.org](http://data.drcog.org).
- Du, M., Li, N., Hu, T., Yang, Q., Chakrabarty, T., Venter, Z., et al. (2024). Daytime cooling efficiencies of urban trees derived from land surface temperature are much higher than those for air temperature. *Environmental Research Letters*, 19, Article 044037. <https://doi.org/10.1088/1748-9326/ad30a3>
- Duncan, J. M. A., Boruff, B., Saunders, A., Sun, Q., Hurley, J., & Amati, M. (2019). Turning down the heat: An enhanced understanding of the relationship between urban vegetation and surface temperature at the city scale. *Science of the Total Environment*, 656, 118–128. <https://doi.org/10.1016/j.scitotenv.2018.11.223>
- Dwyer, J. L., Roy, D. P., Sauer, B., Jenkerson, C. B., Zhang, H. K., & Lymburner, L. (2018). Analysis ready data: enabling analysis of the landsat archive. *Remote Sensing*, 10, 1363. <https://doi.org/10.3390/rs10091363>
- Gann D., Benjamin A., & Hochmair H. (2020). Miami-dade county urban tree cover 2014. [10.34703/GZX1-9V95/QQRWHE](https://doi.org/10.34703/GZX1-9V95/QQRWHE)
- Gardes, T., Schoetter, R., Hidalgo, J., Long, N., Marquès, E., & Masson, V. (2020). Statistical prediction of the nocturnal urban heat island intensity based on urban morphology and geographical factors - An investigation based on numerical model results for a large ensemble of French cities. *Science of The Total Environment*, 737, Article 139253. <https://doi.org/10.1016/j.scitotenv.2020.139253>
- Garrison, J. D. (2021). Environmental justice in theory and practice: Measuring the equity outcomes of Los Angeles and New York's "million trees" campaigns. *Journal of Planning Education and Research*, 41, 6–17. <https://doi.org/10.1177/0739456X18772072>
- Grijseels, N. H., Litvak, E., Avoil, M. L., Bratt, A. R., Cavender-Bares, J., Groffman, P. M., et al. (2023). Evapotranspiration of residential lawns across the United States. *Water Resources Research*, 59, Article e2022WR032893. <https://doi.org/10.1029/2022WR032893>
- Grimmond, C. S. B., Blackett, M., Best, M. J., Barlow, J., Baik, J. J., Belcher, S. E., et al. (2010). The international urban energy balance models comparison project: First results from phase 1. *Journal of Applied Meteorology and Climatology*, 49, 1268–1292. <https://doi.org/10.1175/2010JAMC2354.1>
- Hondula, D. M., Davis, R. E., & Georgescu, M. (2018). Clarifying the connections between green space, urban climate, and heat-related mortality. *American Journal of Public Health*, 108, S62–S63. <https://doi.org/10.2105/AJPH.2017.304295>
- Hu, J., Zhou, Y., Yang, Y., Chen, G., Chen, W., & Hejazi, M. (2023). Multi-city assessments of human exposure to extreme heat during heat waves in the United States. *Remote Sensing of Environment*, 295, Article 113700. <https://doi.org/10.1016/j.rse.2023.113700>
- Ibsen, P. C., Borowy, D., Dell, T., Greydanus, H., Gupta, N., Hondula, D. M., et al. (2021). Greater aridity increases the magnitude of urban nighttime vegetation-derived air cooling. *Environmental Research Letters*, 16, Article 034011. <https://doi.org/10.1088/1748-9326/abdf8a>
- Ibsen, P. C., Crawford, B. R., Corro, L. M., Bagstad, K. J., McNellis, B. E., Jenerette, G. D., et al. (2024). Urban tree cover provides consistent mitigation of extreme heat in arid but not humid cities - data release. *U.S. Geological Survey Data Release*. <https://doi.org/10.5066/P1LIK0C0>
- Ibsen, P. C., Jenerette, G. D., Dell, T., Bagstad, K. J., & Diffendorfer, J. E. (2022). Urban landcover differentially drives day and nighttime air temperature across a semi-arid city. *Science of The Total Environment*, 829, Article 154589. <https://doi.org/10.1016/j.scitotenv.2022.154589>
- Jenerette, G. D., Harlan, S. L., Stefanov, W. L., & Martin, C. A. (2011). Ecosystem services and urban heat riskscape moderation: Water, green spaces, and social inequality in Phoenix, USA. *Ecological Applications*, 21, 2637–2651. <https://doi.org/10.1890/10-1493.1>
- Kim, K., Jung, J., Schollaert, C., & Spector, J. T. (2021). A comparative assessment of cooling center preparedness across twenty-five U.S. Cities. *LJERPH*, 18, 4801. <https://doi.org/10.3390/ljerph18094801>
- Lau, T.-K., Chen, Y.-C., & Lin, T.-P. (2023). Application of local climate zones combined with machine learning to predict the impact of urban structure patterns on thermal environment. *Urban Climate*, 52, Article 101731. <https://doi.org/10.1016/j.ulclim.2023.101731>
- Lenth, R. V. (2016). Least-Squares Means: The R Package lsmeans. *Journal of Statistical Software*, 69, 1–33. <https://doi.org/10.18637/jss.v069.i01>
- Leys, C., Ley, C., Klein, O., Bernard, P., & Licata, L. (2013). Detecting outliers: Do not use standard deviation around the mean, use absolute deviation around the median. *Journal of Experimental Social Psychology*, 49, 764–766. <https://doi.org/10.1016/j.jesp.2013.03.013>
- Li, D., Liao, W., Rigden, A. J., Liu, X., Wang, D., Malyshev, S., et al. (2019). Urban heat island: Aerodynamics or imperviousness? *Science Advances*, 5, eaau4299. <https://doi.org/10.1126/sciadv.aau4299>
- Liaw A., & Wiener M. (2002). Classification and regression by random forest. *R News* 2, 18–22.
- Liu, Y., An, Z., & Ming, Y. (2024). Simulating influences of land use/land cover composition and configuration on urban heat island using machine learning. *Sustainable Cities and Society*, 108, Article 105482. <https://doi.org/10.1016/j.scs.2024.105482>
- Logan, T. M., Zaichik, B., Guikema, S., & Nisbet, A. (2020). Night and day: The influence and relative importance of urban characteristics on remotely sensed land surface temperature. *Remote Sensing of Environment*, 247, Article 111861. <https://doi.org/10.1016/j.rse.2020.111861>
- Lonsdorf, E. V., Nootenboom, C., Janke, B., & Horgan, B. P. (2021). Assessing urban ecosystem services provided by green infrastructure: Golf courses in the Minneapolis-St. Paul metro area. *Landscape and Urban Planning*, 208, Article 104022. <https://doi.org/10.1016/j.landurbplan.2020.104022>
- Maes J., Quaglia A.P., Pereira A.G., Tokarski M., Julian G., Marando F. et al. (2021). BiodiverCities: A roadmap to enhance the biodiversity and green infrastructure of European cities by 2030 : Progress report Publications Office, European Commission. Joint Research Centre, LU.
- Manoli, G., Fatichi, S., Bou-Zeid, E., & Katul, G. G. (2020). Seasonal hysteresis of surface urban heat islands. *Proceedings of the National Academy of Sciences of the United States of America*, 117, 7082–7089. <https://doi.org/10.1073/pnas.1917554117>
- Marchin, R. M., Esperon-Rodriguez, M., Tjoelker, M. G., & Ellsworth, D. S. (2022). Crown dieback and mortality of urban trees linked to heatwaves during extreme drought. *Science of The Total Environment*, 850, Article 157915. <https://doi.org/10.1016/j.scitotenv.2022.157915>
- Mohammad, P., Goswami, A., Chauhan, S., & Nayak, S. (2022). Machine learning algorithm based prediction of land use land cover and land surface temperature changes to characterize the surface urban heat island phenomena over Ahmedabad city, India. *Urban Climate*, 42, Article 101116. <https://doi.org/10.1016/j.ulclim.2022.101116>

- Mullins, J. T., & White, C. (2019). Temperature and mental health: Evidence from the spectrum of mental health outcomes. *Journal of Health Economics*, 68, Article 102240. <https://doi.org/10.1016/j.jhealeco.2019.102240>
- Mushore, T. D., Odindi, J., Dube, T., & Mutanga, O. (2017). Understanding the relationship between urban outdoor temperatures and indoor air-conditioning energy demand in Zimbabwe. *Sustainable Cities and Society*, 34, 97–108. <https://doi.org/10.1016/j.scs.2017.06.007>
- Offerle, B., Grimmond, C. S. B., & Fortuniak, K. (2005). Heat storage and anthropogenic heat flux in relation to the energy balance of a central European city centre. *International Journal of Climatology*, 25, 1405–1419. <https://doi.org/10.1002/joc.1198>
- Oke, T. R. (1982). The energetic basis of the urban heat island. *Quarterly Journal of the Royal Meteorological Society*, 108, 1–24. <https://doi.org/10.1002/qj.49710845502>
- Oke, T. R., Mills, G., Christen, A., & Voogt, J. A. (2017). *Urban climates*. Cambridge: Cambridge University Press. <https://doi.org/10.1017/9781139016476>
- Omernik, J. M., & Griffith, G. E. (2014). Ecoregions of the Contiguous United States: Evolution of a Hierarchical Spatial Framework. *Environmental Management*, 54, 1249–1266. <https://doi.org/10.1007/s00267-014-0364-1>
- Ossola, A., & Lin, B. B. (2021). Making nature-based solutions climate-ready for the 50 °C world. *Environmental Science & Policy*, 123, 151–159. <https://doi.org/10.1016/j.envsci.2021.05.026>
- Park, Y., Guldmann, J.-M., & Liu, D. (2021). Impacts of tree and building shades on the urban heat island: Combining remote sensing, 3D digital city and spatial regression approaches. *Computers, Environment and Urban Systems*, 88, Article 101655. <https://doi.org/10.1016/j.compenvurbsys.2021.101655>
- Pebesma, E. J. (2004). Multivariable geostatistics in S: The gstat package. *Computers and Geosciences*, 30, 683–691. <https://doi.org/10.1016/j.cageo.2004.03.012>
- Pilant, A., Endres, K., Rosenbaum, D., & Gundersen, G. (2020). US EPA enviroatlas meter-scale urban land cover (MULC): 1-m pixel land cover class definitions and guidance. *Remote Sensing*, 12, 1909. <https://doi.org/10.3390/rs12121909>
- Pima county geospatial data portal [WWW document], (2023). URL <https://gisopendata.pima.gov/>.
- PRISM Group, (2007). PRISM climate group [WWW document]. URL <http://www.prism.oregonstate.edu/>.
- Rahman, M. A., Dervishi, V., Moser-Reischl, A., Ludwig, F., Pretzsch, H., Rötzer, T., et al. (2021). Comparative analysis of shade and underlying surfaces on cooling effect. *Urban Forestry and Urban Greening*, 63. <https://doi.org/10.1016/j.ufug.2021.127223>
- Rahman, M. A., Hartmann, C., Moser-Reischl, A., von Strachwitz, M. F., Paeth, H., Pretzsch, H., et al. (2020). Tree cooling effects and human thermal comfort under contrasting species and sites. *Agricultural and Forest Meteorology*, 287, Article 107947. <https://doi.org/10.1016/j.agrformet.2020.107947>
- Romitti, Y., Sue Wing, I., Spangler, K. R., & Wellenius, G. A. (2022). Inequality in the availability of residential air conditioning across 115 US metropolitan areas. *PNAS Nexus*, 1, pgac210. <https://doi.org/10.1093/pnasnexus/pgac210>
- Schumacher, D. L., Hauser, M., & Seneviratne, S. I. (2022). Drivers and mechanisms of the 2021 pacific northwest heatwave. *Earth's Future*, 10. <https://doi.org/10.1029/2022EF002967>
- Shandas, V., Voelkel, J., Williams, J., & Hoffman, J. (2019). Integrating satellite and ground measurements for predicting locations of extreme urban heat. *Climate*, 7, 1–13. <https://doi.org/10.3390/cli7010005>
- Shashua-Bar, L., Rahman, M. A., Moser-Reischl, A., Peeters, A., Franceschi, E., Pretzsch, H., et al. (2023). Do urban tree hydraulics limit their transpirational cooling? A comparison between temperate and hot arid climates. *Urban Climate*, 49, Article 101554. <https://doi.org/10.1016/j.uclim.2023.101554>
- Shi, R., Hobbs, B. F., Zaitchik, B. F., Waugh, D. W., Scott, A. A., & Zhang, Y. (2021). Monitoring intra-urban temperature with dense sensor networks: Fixed or mobile? An empirical study in Baltimore, MD. *Urban Climate*, 39, Article 100979. <https://doi.org/10.1016/j.uclim.2021.100979>
- Shiflett, S. A., Liang, L. L., Crum, S. M., Feyisa, G. L., Wang, J., & Jenerette, G. D. (2017). Variation in the urban vegetation, surface temperature, air temperature nexus. *Science of The Total Environment*, 579, 495–505. <https://doi.org/10.1016/j.scitotenv.2016.11.069>
- Smith, I. A., Fabian, M. P., & Hutyra, L. R. (2023). Urban green space and albedo impacts on surface temperature across seven United States cities. *Science of The Total Environment*, 857, Article 159663. <https://doi.org/10.1016/j.scitotenv.2022.159663>
- Snyder G.I. (2012). The 3D Elevation Program: Summary of program direction (Report No. 2012–3089. Reston, VA: Fact Sheet. [10.3133/fs20123089](https://doi.org/10.3133/fs20123089)
- Sulman, B. N., Roman, D. T., Yi, K., Wang, L., Phillips, R. P., & Novick, K. A. (2016). High atmospheric demand for water can limit forest carbon uptake and transpiration as severely as dry soil. *Geophysical Research Letters*, 43, 9686–9695. <https://doi.org/10.1002/2016GL069416>
- Terando, A. J., Youngsteadt, E., Meineke, E. K., & Prado, S. G. (2017). Ad hoc instrumentation methods in ecological studies produce highly biased temperature measurements. *Ecology and Evolution*, 7, 9890–9904. <https://doi.org/10.1002/ece3.3499>
- Thompson, V., Kennedy-Asser, A. T., Vosper, E., Lo, Y. T. E., Huntingford, C., Andrews, O., et al. (2022). The 2021 western North America heat wave among the most extreme events ever recorded globally. *Science Advances*, 8, 1–11. <https://doi.org/10.1126/sciadv.abm6860>
- Tian, W., Yang, Y., Wang, L., Zong, L., Zhang, Y., & Liu, D. (2023). Role of local climate zones and urban ventilation in canopy urban heat island–heatwave interaction in Nanjing megacity, China. *Urban Climate*, 49, Article 101474. <https://doi.org/10.1016/j.uclim.2023.101474>
- United State White House, (2023). Biden administration mobilizes to protect workers and communities from extreme heat [Fact sheet].
- Winbourne, J. B., Jones, T. S., Garvey, S. M., Harrison, J. L., Wang, L., Li, D., et al. (2020). Tree transpiration and urban temperatures: Current understanding, implications, and future research directions. *Bioscience*, 70, 576–588. <https://doi.org/10.1093/biosci/biaa055>
- Yuan, W., Zheng, Y., Piao, S., Ciais, P., Lombardozzi, D., Wang, Y., et al. (2019). Increased atmospheric vapor pressure deficit reduces global vegetation growth. *Science Advances*, 5, 1–14. <https://doi.org/10.1126/sciadv.aax1396>
- Zhou, W., Huang, G., Pickett, S. T. A., Wang, J., Cadenasso, M. L., McPhearson, T., et al. (2021). Urban tree canopy has greater cooling effects in socially vulnerable communities in the US. *One Earth*, 4, 1764–1775. <https://doi.org/10.1016/j.oneear.2021.11.010>
- Ziter, C. D., Pedersen, E. J., Kucharik, C. J., & Turner, M. G. (2019). Scale-dependent interactions between tree canopy cover and impervious surfaces reduce daytime urban heat during summer. *Proceedings of the National Academy of Sciences of the United States of America*, 116, 7575–7580. <https://doi.org/10.1073/pnas.1817561116>